Use of complex frequency plane to design broadband and sub-wavelength absorbers

V. Romero-García, G. Theocharis, O. Richoux, and V. Pagneux

Citation: The Journal of the Acoustical Society of America **139**, 3395 (2016); doi: 10.1121/1.4950708
View online: https://doi.org/10.1121/1.4950708
View Table of Contents: https://asa.scitation.org/toc/jas/139/6
Published by the Acoustical Society of America

Use of complex frequency plane to design broadband and sub-wavelength absorbers

V. Romero-García,[a] G. Theocharis, O. Richoux, and V. Pagneux
LUNAM Université, Université du Maine, Laboratoire d'Acoustique de l'Université du Maine UMR CNRS 6613 (LAUM), Av. O. Messiaen, 72085 Le Mans, France

(Received 20 October 2015; revised 17 January 2016; accepted 14 February 2016; published online 30 June 2016)

The reflection of sound of frequency below 1 kHz, by a rigid-backed structure that contains sub-wavelength resonators is studied in this work. In particular, only single mode reflected waves are considered, an approximation which is accurate in this low frequency regime. A method of analysis of absorption that uses the structure of the reflection coefficient in the complex frequency plane is proposed. In the absence of losses, the reflection coefficient supports pairs of poles and zeros that are complex conjugate and which have imaginary parts linked to the energy leakage by radiation. When losses are introduced and balanced to the leakage, the critical coupling condition is satisfied and total absorption is obtained. Examples of a slot resonator and of multiple Helmholtz resonators are analyzed to obtain both narrow and broadband total absorption. © *2016 Acoustical Society of America*. [http://dx.doi.org/10.1121/1.4950708]

[MRH] Pages: 3395–3403

I. INTRODUCTION

In acoustics the control of noise is of particular interest leading to the design of new materials and structures for different applications: room acoustics,[1] duct mufflers,[2] urban and environmental acoustics,[3,4] acoustic medical devices,[5] and high amplitude scattering (launch fairings,[6] for example). Among all these applications, absorption of audible sound takes an important position since excessive noise exposure becomes a major public health concern. Thus, thin and lightweight absorbers that are both easily installed and capable to absorb sound over a wide frequency range are strongly desired.

Numerous works deal with the design of new structured materials to improve the sound absorption for a large range of frequencies and different solutions have been implemented to achieve this purpose (for a review see Ref. 7). For audible frequencies above 1 kHz, porous materials as thin as 10 cm are excellent candidates to achieve this goal.[8] Nevertheless, most irritating noise belongs to the low frequency regime (in audible frequencies typically below 1 kHz), where thin porous materials are inefficient. Structures based on sub-wavelength resonances provide an ideal solution to design thin and low frequency absorbing materials.

As an example, the combination of porous materials with backed structures like tunable cavities,[8] perforated plates,[9] Helmholtz resonators,[10] or rigid multi-irregularities gratings[11] show excellent absorption properties in the low frequency range. Similarly, Helmholtz resonator panels,[12] panels of Schroeder diffusers combined with perforated plates,[7] perforated plates combined with tunable cavities[13–15] or Helmholtz resonators,[16] sonic crystals slabs with resonant scatterers[17–20] or periodic groove structures[21] can be excellent alternative solutions to achieve efficient sound absorbing structures in the low frequency regime. A very efficient solution is also to use micro-perforations instead of porous materials[22] or slow sound structures.[23,24]

In most of these applications, the common solution to enhance the frequency broadness of the low-frequency absorption is to build unit cells with frequency-overlapped resonant modes (each of them with an absorption peak close to one). So, the achievement of very efficient low-frequency, broadband absorption is the result of a fine tuning of the attenuation properties with resonances characteristics of the structure that leads to the critical coupling of the resonant modes.[25–27]

This work introduces the complex frequency plane of the reflection coefficient as an efficient tool to design broadband acoustic absorbers in the low frequency range. Other approaches based on the Smith chart have been used in solving problems with transmission lines or matched systems in electronics for the radio frequency.[28–30] In our case, fine tuning of the losses and of the geometric characteristics of the sub-wavelength resonators leads to the crossing of the complex zeros of the reflection coefficient with the real axis which signifies the perfect absorption condition.[31] The paper is constructed as follows: first, the simple case of a slot which is a quarter wavelength resonator is presented. Very simple analytical expressions of the complex zero and pole of the reflection coefficient are derived for small radiation leakage and small losses. Then, it is shown that the addition of a purely resistive coating at the back of the slot can lead to perfect absorption. Second, the case of a lossy Helmholtz resonator (HR) loaded at the end of a waveguide is studied using an analytical calculation for the case of the weak coupling of the HR with the waveguide (perturbative regime) and using numerical simulation for the strong coupling case. As a result, the stronger the coupling of the HR with the waveguide is, the broader the absorption peak is. Finally,

[a]Electronic mail: virogar1@mat.upv.es

using the complex frequency plane method, a broadband perfect absorber is designed by arranging four properly tuned HRs.

II. COMPLEX FREQUENCY PLANE

This section introduces the concept of the zeros and the poles of the reflection coefficient in the complex frequency plane as a tool to interpret the perfect absorption. It starts with the simple case of a slot which is related with the concept of coiling up space for constructing sub-wavelength acoustic metamaterials. Then the complexity of the analysis is increased by studying the case of the HR, widely used in the literature of acoustic metamaterials. A toy model is developed to obtain analytical expressions of the complex frequencies of the zeros and poles of the reflection coefficient for these systems in the perturbative regime. The section ends with a realistic case, considering the full expression for the viscothermal losses in the walls of the resonators and adding porous materials.

A. Simple case: Slot resonator

Consider the simple case of a slot with a quarter wavelength resonance. Since the interest is in the low frequency regime, only single-mode reflected waves are considered. In other words, attention is paid to the range of frequencies, f, smaller than the cutoff frequency of the waveguide; therefore the problem can be considered as 1D. This one-mode approximation allows us to illustrate with very simple analytic expressions the appearance of the zeros and poles of the reflection coefficient. The geometry of interest is displayed in Fig. 1(a): it corresponds both to an incident wave on a slot of length L and section S_2 at the end of a waveguide of section S_1 or to a wave normally incident on a wall with periodic slots. The slot may be coiled as shown in Fig. 1(b) to become a sub-wavelength resonator.

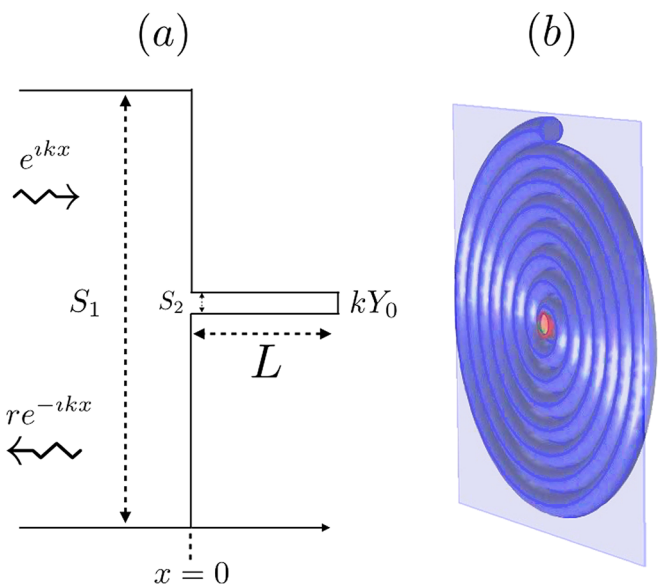

FIG. 1. (Color online) (a) Scheme of the slot. (b) Representation of the slot using the concept of coiling up space.

In this paper, the time dependence convention of the harmonic regime is $e^{-\imath\omega t}$, and it will be omitted in the following. A plane wave is incident from the left such that an standing wave of the form

$$p = e^{\imath kx} + re^{-\imath kx} \tag{1}$$

is created in $x<0$. The wavenumber is $k=\omega/c$ with c the acoustic wave speed and r is the reflection coefficient.

1. Lossless case

For a rigid wall at the end of the slot $p'(L)=0$ and thus $p'(0^+)/p(0^+) = k\tan(kL)$, with the prime denoting differentiation with respect to x. Then, assuming a one-mode approximation, the continuity conditions are $p(0^-)=p(0^+)$ and $S_1p'(0^-)=S_2p'(0+)$. That leads to the expression of the reflection coefficient,

$$r = \frac{\cot(kL) + \imath\, S_2/S_1}{\cot(kL) - \imath\, S_2/S_1}. \tag{2}$$

For a real frequency (k real), $|r|=1$ is recognized as dictated by energy conservation. Going to the complex frequency plane (complex k), Eq. (2) shows that r satisfies $\overline{r(k)} = 1/r(\bar{k})$ where $\overline{r(k)}$ and $\bar{k}$ represent the complex conjugate of $r(k)$ and k, respectively. The reflection coefficient has pairs of poles and zeros that are complex conjugate, where the poles have a negative imaginary part and the zeros have a positive imaginary part. These properties are general;[33] they come from the structure of the wave equation (Helmholtz equation) and are not dependent on the one-mode approximation used in this calculation. Note nevertheless that the sign of the imaginary parts of poles and zeros depend on the time convention, here $e^{-\imath\omega t}$.

From Eq. (2), the poles correspond to $\cot(kL) - \imath\, S_2/S_1 = 0$ and the zeros to $\cot(kL) + \imath\, S_2/S_1 = 0$. Assuming that the slot is thin ($S_2/S_1 \ll 1$), the expression of the first pole-zero pair is given by

$$(kL)_{\text{pole}} = \frac{\pi}{2} - \imath\frac{S_2}{S_1}, \tag{3}$$

$$(kL)_{\text{zero}} = \frac{\pi}{2} + \imath\frac{S_2}{S_1}. \tag{4}$$

Next pairs of pole-zero are just shifted by $m\pi$ ($m\geq 1$) and will not be regarded in the following. The complex pole of Eq. (3) corresponds to a complex resonance frequency of the slot with an open end at $x=0$. The imaginary part (S_2/S_1) represents the leakage due to the radiation at the open end toward the exterior of the slot. With the convention of time dependence used in this work, the wave at the resonance frequency decreases as $e^{Im(\omega^{pole})t}$ [where $\omega^{\text{pole}} = (kL)_{\text{pole}}c/L$], thus the decay time, τ_{leak}, can be related with the quality factor due to the leakage as,

$$Q_{\text{leak}} = \frac{Re(\omega_{\text{pole}})\tau_{\text{leak}}}{2} = \frac{Re(\omega_{\text{pole}})}{2\text{Im}(\omega_{\text{pole}})}, \tag{5}$$

where the leakage rate can be defined as $\Gamma_{\text{leak}} = 1/\tau_{\text{leak}} = \text{Im}(\omega_{\text{pole}})$. The $|r|$ in the complex frequency plane is shown

in Fig. 2(a). According to the theory, there is a pole with negative imaginary part and a zero which is its complex conjugate. In the neighborhood of the pole-zero pair, r is just given by $r = (kL - \pi/2 - \imath S_2/S_1)/(kL - \pi/2 + \imath S_2/S_1)$. Consequently, for real frequency (k real), although $|r| = 1$, the complex resonance frequency is seen as a rapid phase change of the reflection coefficient around $kL = \pi/2$. The imaginary part, which is related with the leakage rate of energy from the slot to the surrounding space, is equal to S_2/S_1, and it gives the quality factor of this rapid phase change.

2. Lossy case

Now a lossy coating at the end of the slot, such that $p'(L) = kY_0\,p(L)$ where $\mathrm{Im}(Y_0) > 0$ is considered. The reduced admittance Y_0 has a positive imaginary part that corresponds to the loss of the coating. By using $p'(0^+)/p(0^+) = (k\tan(kL) + p'(L)/p(L))(1 - \tan(kL)/k \times p'(L)/p(L))$, the reflection coefficient is changed from Eq. (2) to

$$r = \frac{\cot(kL) - Y_0 + \imath\, S_2/S_1(1 + Y_0\cot(kL))}{\cot(kL) - Y_0 - \imath\, S_2/S_1(1 + Y_0\cot(kL))}. \tag{6}$$

Because of the loss ($\mathrm{Im}(Y_0) > 0$), $|r| < 1$ for real frequency k. Besides, the pole-zero pair is now shifted in the complex k plane. For thin slot and small coating ($Y_0 = O(S_2/S_1) \ll 1$), the pair is given analytically by

$$(kL)_{\mathrm{pole}} = \frac{\pi}{2} - \imath\frac{S_2}{S_1} - Y_0, \tag{7}$$

$$(kL)_{\mathrm{zero}} = \frac{\pi}{2} + \imath\frac{S_2}{S_1} - Y_0. \tag{8}$$

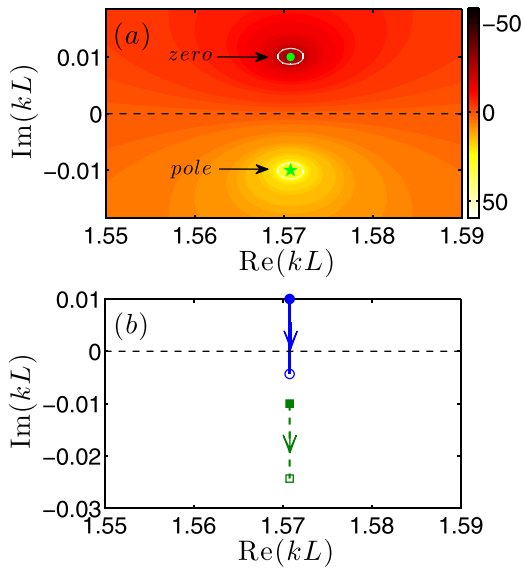

FIG. 2. (Color online) Analysis of the complex plane for the slot. (a) Representation of the 20 $\log(|r|)$ in the complex frequency plane for the lossless case. The analyzed slot has the following parameters $L = 25$ cm, $S_2/S_1 = 0.1$. The dot and the star represent the zero and the pole, respectively, obtained considering the low frequency approximation [Eqs. (3) and (4)]. (b) Dependence of the complex frequency of the zero (continuous line) and the pole (dashed line) on the losses added to the system. Arrows show the direction of the trajectory of the pole as the losses are increased. Filled symbols represent the lossless case and open symbols represent the last considered lossy case.

By comparing Eqs. (3) and (4) and Eqs. (7) and (8) the effect of the lossy coating is explicit: the pole and the zero are shifted downward in the complex frequency plane by Y_0. This shift is illustrated in Fig. 2(b) for a purely resistive admittance $Y_0 = \imath A$ with $A > 0$.

From the point of view of absorption defined as $\alpha = 1 - |r|^2$, all that has decisive consequences: the zero of r coincides with the real frequency axis (k real) of the complex plane when

$$S_2/S_1 = \mathrm{Im}(Y_0). \tag{9}$$

Then, there is total absorption (for a real frequency) and it corresponds to the critical coupling where the leakage (S_2/S_1) is balanced by the loss ($\mathrm{Im}(Y_0)$). It is worthwhile to emphasize here that the narrowband or broadband character of this absorption peak is only governed by the radiation leakage through the distance between the pole and the zero in the complex frequency plane. The loss just shifts the pole-zero pair [see the differences between Eqs. (3) and (4) and Eqs. (7) and (8)].

B. Helmholtz resonator

Now, the case of a closed cylindrical waveguide filled with air and loaded with a HR at the end of the waveguide is considered (see Fig. 3). The waveguide has a section S_t, while the HR is composed of a cylindrical neck, with section S_n and length l_n, and a cylindrical cavity, with section S_c and length l_c. As before, a plane wave is incident from the left. Once again, the one-mode approximation is considered since attention is paid in the range of frequencies, f, smaller than the cutoff frequency of the waveguide. The reflection coefficient of this system reads as

$$r = \frac{Z_{HR} - 1}{Z_{HR} + 1}, \tag{10}$$

where Z_{HR} is the normalized impedance of the HR with respect to the characteristic impedance of the waveguide, Z_t.

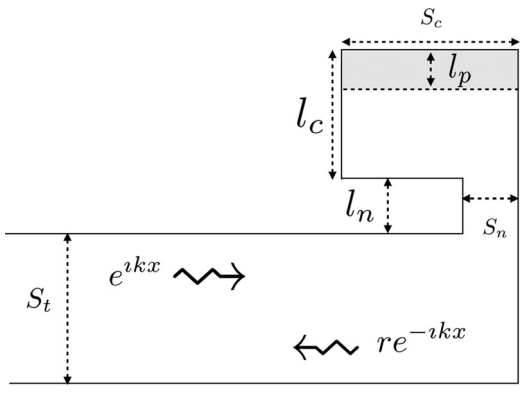

FIG. 3. Scheme of the system made of a HR parallel loaded to a waveguide filled with air. The waveguide has a cross section S_t, while the HR is characterized by a neck, with cross section S_n and length l_n, and a cavity, with cross section S_c and length of l_c. Eventually, a layer of porous material of thickness l_p can be considered. The incident wave, $e^{\imath kx}$ propagates in the waveguide and reflected wave, $re^{-\imath kx}$, is produced by the presence of the HR and the rigid termination.

The normalized impedance of the HR is given by the following expression,[32]

$$Z_{HR} = \imath \frac{Z_n}{Z_t} \frac{Z_c/Z_n - \tan(k_c l_c)\tan(k_n l_n)}{(Z_c/Z_n)\tan(k_n l_n) + \tan(k_c l_c)}, \tag{11}$$

where Z_i, k_i are the characteristic impedances and wavenumbers of each part of the system with $i = t$ for the waveguide, $i = n$ for the neck, and $i = c$ for the cavity of the HRs.

1. Lossless case

In the lossless low frequency limit, one can consider that $k_i l_i \ll 1$ and $k_i = k = \omega/c$ with $Z_i = \rho c/S_i$ (where $S_i = \pi R_i^2$ are the cross sections of each part of the system and ρ the density of air). In this case the impedance of the HR reads as

$$Z_{HR}^{LF} = \imath\beta\left(\frac{k_{HR}^2 - k^2}{k}\right), \tag{12}$$

with

$$\beta = \frac{l_c l_n}{\frac{S_n}{S_t}\left(\frac{S_n}{S_c} l_n + l_c\right)}, \tag{13}$$

$$k_{HR} = \sqrt{\frac{S_n}{S_c l_c l_n}}, \tag{14}$$

where k_{HR} is the resonance wavenumber of the HR and β is a parameter related with the leakage. By substituting Eq. (12) in Eq. (10), the following complex frequencies of the zeros, $k_{\text{zero}}^{\text{lossless}}$, and poles, $k_{\text{pole}}^{\text{lossless}}$, of the reflection coefficient are found

$$k_{\text{zero}}^{\text{lossless}} = \sqrt{k_{HR}^2 - \frac{1}{4\beta^2}} + \imath\frac{1}{2\beta}, \tag{15}$$

$$k_{\text{pole}}^{\text{lossless}} = \sqrt{k_{HR}^2 - \frac{1}{4\beta^2}} - \imath\frac{1}{2\beta}. \tag{16}$$

As explained above, the zero and the pole are complex conjugates. The imaginary part of the complex frequency of the pole is related with the leakage rate of energy from the resonator to the waveguide defined as $\Gamma_{\text{leak}} = \text{Im}(\omega_{\text{pole}}) = c/2\beta$. The real part of the complex frequency of the zero (or the pole) is related with the resonance frequency of the system. However, the real part of this complex resonance depends also on the leakage between the HR and the waveguide.

Figure 4(a) represents the reflection coefficient in the complex frequency plane for a specific HR having a small leakage rate, i.e., weak coupling with the waveguide (see Fig. 4 for more details). Since we study the lossless case, the reflection coefficient in the real frequency axis is 1 for all the frequencies. The color map shows the reflection coefficient calculated from the whole expression of r, Eq. (10), while the dot and star represent the zero and the pole in the low frequency approximation from the Eqs. (15) and (16), respectively.

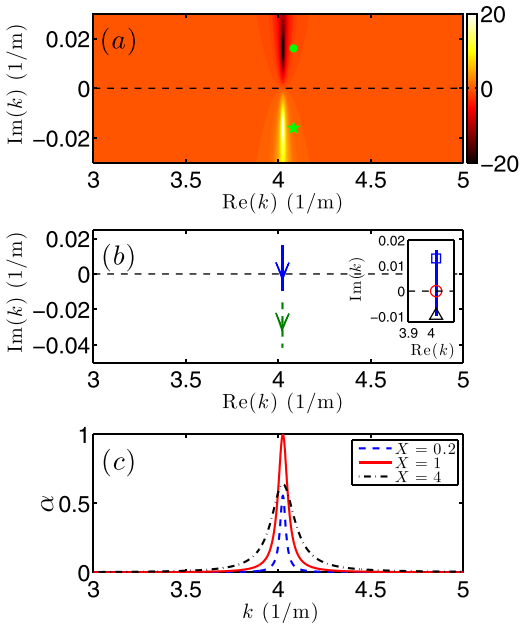

FIG. 4. (Color online) Analysis of the complex plane for a weak coupling between the HR and the waveguide (small leakage). (a) Representation of the 20 $\log(|r|)$ in the complex frequency plane for the lossless case. The analyzed HR has the following parameters $S_t = 314\,\text{cm}^2$, $l_n = 4\,\text{cm}$, $l_c = 6\,\text{cm}$, $S_n = 0.39\,\text{cm}^2$, $S_c = 9.8\,\text{cm}^2$. The dot and the star represent the zero and the pole obtained considering the low frequency approximation [Eqs. (15) and (16)]. (b) Dependence of the complex frequency of the zero (continuous line) and the pole (dashed line) on the losses added to the system. Arrows show the direction of the trajectory of both the zero and the pole as the losses are increased. (c) Evaluation of the absorption coefficient of three different configurations with different amount of losses. Symbols in the inset of (b), i.e., blue square, red circle and black triangle represent the position of the zero on the three configurations analyzed in (c).

2. Lossy case

The presence of losses in the system generally induces a real part in the impedance of the system. This real part will be introduced for example, by adding a lossy coating at the end of the HR, as it is previously done for the case of the slot, or by considering the viscothermal losses into the system. Here, for simplicity, the toy model is built using a constant real part, X, in the impedance of the HR [Eqs. (11) and (12)]. In the low frequency limit, and considering weak leakage between the HR and the waveguide, the zero and the pole read as

$$k_{\text{zero}}^{\text{lossy}} = k_{HR} + \imath\frac{1}{2\beta}(1 - X), \tag{17}$$

$$k_{\text{pole}}^{\text{lossy}} = k_{HR} - \imath\frac{1}{2\beta}(1 + X). \tag{18}$$

Figures 4(b) represents the shift of the zero of the reflection coefficient by adding losses into the HR. Both the zero and the pole are down shifted as shown by Eqs. (17) and (18). Interestingly, for the case in which $X = 1$, i.e., when the impedance matching is fulfilled, the zero of the reflection coefficient crosses the real axis. This happens when the loss

factor added to the system, $X/2\beta$, is exactly the leakage of the HR. Once again, this is the well known critical coupling condition. Figure 4(c) represents the absorption coefficient for three different cases analyzing the two extreme cases of small and large losses as well as the balanced case (critical coupling). When the losses balance the leakage of the HR, the imaginary part is zero and the real part coincides with the resonant frequency of the HR producing perfect absorption. It is worth noting here that for the case $X=4$, in which the losses are much bigger than in the critical coupling condition, this nonintuitive result is due to the non balanced leakage with respect to the inherent losses of the system.

Now, we turn to the case of strong leakage between the HR and the waveguide (see caption of Fig. 5 for details about the HR parameters). In the low frequency limit, the zero and the pole read as

$$k_{\text{zero}}^{\text{lossy}} = \sqrt{k_{HR}^2 - \frac{(1-X)^2}{4\beta^2}} + \imath\frac{1}{2\beta}(1-X), \tag{19}$$

$$k_{\text{pole}}^{\text{lossy}} = \sqrt{k_{HR}^2 - \frac{(1-X)^2}{4\beta^2}} - \imath\frac{1}{2\beta}(1+X). \tag{20}$$

Figure 5(a) shows the pole and zero in the complex frequency plane in the lossless case. Note that the main difference with respect to the case with small leakage is that now the resonance presents larger imaginary part of the zero and the pole. Figure 5(b) represents the shift of the zero and pole of the reflection coefficient by adding losses into the HR. Again for the case in which $X=1$ the zero of the reflection coefficient reaches the real axis activating the condition of perfect absorption. In this case, the main difference with respect to the small leakage case is that the real part of the zero presents a second order correction. Figure 5(c) represents the absorption coefficient for three different cases analyzing the two extreme cases of small and large losses as well as the balanced case. Notice here that, as the lossless resonant modes have more leakage than in the previous case analyzed in Fig. 4, the absorption peaks become broader.

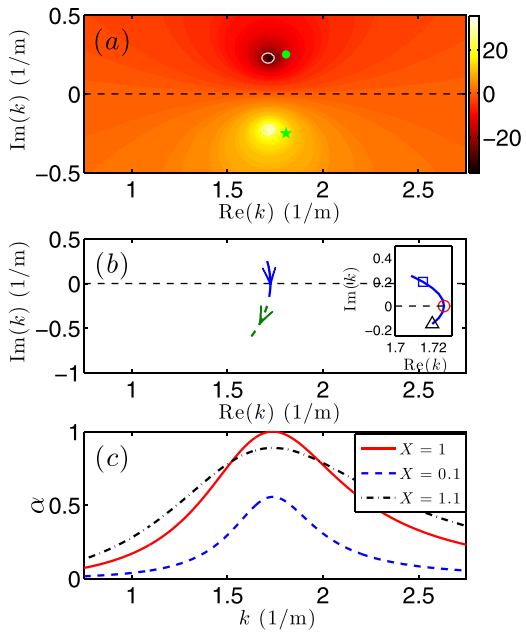

FIG. 5. (Color online) Analysis of the complex plane for a strong coupling between the HR and the waveguide. (a) Representation of the $20\log(|r|)$ in the complex frequency plane for the lossless case. The analyzed HR has the following parameters $S_t=314\,\text{cm}^2$, $l_n=4\,\text{cm}$, $l_c=30\,\text{cm}$, $S_n=6.3\,\text{cm}^2$, $S_c=157\,\text{cm}^2$. The dot and the star represent the zero and pole obtained considering the low frequency approximation [Eqs. (19) and (20)]. (b) Dependence of the complex frequency of the zero (continuous line) and the pole (dashed line) on the losses added to the system. Arrows show the direction of the trajectory both of the zero and the pole as the losses are increased. (c) Evaluation of absorption coefficient of three different configurations with different amount of losses. Symbols in the inset of (b), i.e., blue square, red circle, and black triangle represent the position of the zero on the three configurations analyzed in (c).

C. Realistic case: Lossy HR with porous material

In Sec. II B, we introduced a toy model that takes into account the losses in the HR by adding a real, constant part on the HR impedance. Now, we deal with a more realistic model by considering both the viscothermal losses in the HR and the possibility to introduce a porous layer of length l_p at the end of the cavity of the HR is considered (see gray region in Fig. 3).

Viscothermal losses in the HR are taken into account by considering a complex expression for the acoustic wave number in the neck and in the cavity. The losses are modeled by using Ref. 34, namely, the wave number and the impedances are replaced by the following expressions

$$k_i = \frac{\omega}{c}\left(1+\frac{\kappa}{s_i}\left(1+(\gamma-1)/\chi\right)\right), \tag{21}$$

$$Z_i = \frac{\rho c}{S_i}\left(1+\frac{\kappa}{s_i}\left(1-(\gamma-1)/\chi\right)\right), \tag{22}$$

by setting $s_i = R_i/\delta$ where R_i the radius considered in each tube and $\delta=\sqrt{2\mu/\rho_0\omega}$ the viscous boundary layer thickness with μ being the viscosity of air. $\chi=\sqrt{P_r}$ with P_r the Prandtl number at atmospheric pressure, $\kappa=(1+\imath)/\sqrt{2}$ and $\gamma=1.4$ the heat capacity ratio of air. On the other hand, the length correction of the HR is coming from the addition of two correction lengths $\Delta l = l_1^{corr}+l_2^{corr}$, which are given by[35,36]

$$l_1^{corr} = 0.82[1-1.35R_n/R_c+0.31(R_n/R_c)^3]R_n, \tag{23}$$

$$l_2^{corr} = 0.82[1-0.235R_n/R_t-1.32(R_n/R_t)^2 + 1.54(R_n/R_t)^3-0.86(R_n/R_t)^4]R_n. \tag{24}$$

The length correction of Eq. (23) is due to the pressure radiation at the discontinuity from the neck to the cavity of the HR,[36] while the length correction of Eq. (24) is due to the radiation at the discontinuity from the neck to the principal waveguide.[35]

The wave propagation in the porous layer will be described by the classical Johnson, Champoux, Allard, and Lafarge model[8] that introduces the effective complex wave number, k_p, and impedance, Z_p, of the porous material. The physical parameters used in this work for the properties of

air (viscosity η, specific heat ratio γ, Prandtl number Pr, static pressure of the fluid at rest P_0 and kinematic viscosity of air, μ) and for the macroscopic parameters of the porous medium (porosity ϕ, tortuosity α_∞, air flow resistivity σ, viscous characteristic length Λ, and thermal characteristic length Λ') are shown in Table I. These parameters correspond to Glass wool.[8,37]

With all the previous elements, the normalized impedance of the HR with the layer of porous material, can be obtained as

$$Z_{HRP} = \imath \frac{Z_n}{Z_t} \times \frac{1 - \frac{Z_c}{Z_p} t_c t_p - \frac{Z_n}{Z_c} t_n t_c - \frac{Z_n}{Z_p} t_p t_n - k\Delta l Z_n \left(\frac{t_c}{Z_c} + \frac{t_p}{Z_p} \right)}{t_n - \frac{Z_c}{Z_p} t_c t_p t_n + \frac{Z_n}{Z_c} t_c + \frac{Z_n}{Z_p} t_p - k\Delta l Z_n \left(\frac{t_c t_n}{Z_c} + \frac{t_p t_n}{Z_p} \right)}, \tag{25}$$

where the notation $t_i = \tan(k_i l_i)$ with $i = n, c, t, p$ is used. Notice that Eq. (11) is recovered by setting $l_p = 0$ m (no porous material) and $\Delta l = 0$ m (no length correction).

By using Eq. (25), the reflection coefficient is evaluated in the complex frequency plane. Figure 6(a) represents the pole and the zero of the reflection coefficient by considering only the viscothermal losses in the problem, i.e., by considering $l_p = 0$ m. For the chosen HR (see Fig. 6 for more details), the viscothermal losses are not enough to shift the zero to the real axis and produce perfect absorption. Thus, an additional amount of losses have to be added, for example, by adding porous material, to reach the perfect absorption. Figure 6(c) shows the trajectory of the zero (continuous line) and the pole (dashed line) as the thickness of the porous layer is increased. The configuration at which the zero is in the real axis, the complex frequency plane is shown in Fig. 6(b). In this case the analysis is out of the perturbative regime, therefore the trajectories of the zero and pole in the complex plane are more complicated than the ones obtained with the toy model in Sec. II B 2.

The real part of the impedance that is responsible for the losses in the system can be defined as $X = Re(Z(_{HRP}(\omega_z)))$. Figure 6(d) represents the absorption coefficient for the case without porous material (dashed line), for the perfect absorption (red continuous line) and for a case with large losses (more than the needed ones for the perfect absorption). Again, the condition $X = 1$ is accomplished for the perfect absorption case.

TABLE I. Properties of air and macroscopic properties of porous layer (meter–kilogram–second system).

Air properties at normal conditions		Macroscopic parameters of the porous material	
η	$1.983\ 10^{-5}$ kg/m s	ϕ	0.7
γ	1.4	α_∞	1
Pr	0.702	σ	$1\,100\,000$ Nm^{-4}s
P_0	101 320 N/m^2	Λ	$10\ 10^{-6}$ m
μ	$15.68\ 10^{-6}$ m^2/s	Λ'	$20\ 10^{-6}$ m

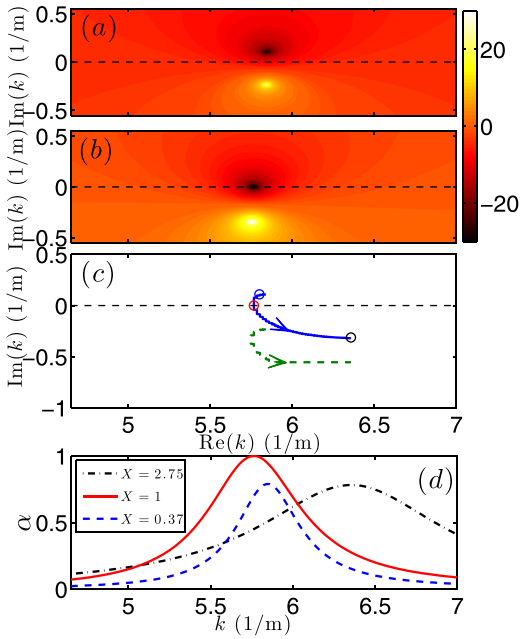

FIG. 6. (Color online) Analysis of the complex plane for a realistic case. The analyzed HR has the following parameters $S_t = 314$ cm^2, $l_n = 1.5$ cm, $l_c = 8$ cm, $S_n = 0.57$ cm^2, $S_c = 9.8$ cm^2. (b) Representation of the $20\log(|r|)$ in the complex frequency plane only considering the viscothermal losses, ($l_p = 0$ mm, $X = 0.37$). (b) Representation of the $20\log(|r|)$ in the complex frequency plane for the critical coupled case, ($l_p = 7.75$ mm, $X = 1$). (c) Trajectories of the zero (continuous line) and of the pole (dashed line) in the complex frequency plane as the porous layer increases. (d) Evaluation of the absorption coefficient for different configurations. Dashed line represents the case without porous material, therefore considering only the viscothermal losses in the tubes. Continuous line corresponds to the critically couple case, with a porous layer of $l_p = 7.75$ mm. Dot dashed line represents the case with large losses in the system introduced by a porous layer of $l_p = 2$ cm.

III. BROADBAND ABSORPTION BY COUPLING PERFECT ABSORPTION PEAKS

This section describes the possibility to design broadband absorbers by using multiple critically coupled resonances. In particular, a structure analogous to the one used in Sec. II, but now having four HRs loaded to the cylindrical closed waveguide is considered. A side view of the setup is shown in Fig. 7. In this system the total impedance can be obtained by

$$\frac{1}{Z_{\text{total}}} = \sum_{n=1}^{4} \frac{1}{Z^n_{HRP}}, \tag{26}$$

where Z^n_{HRP} is the impedance of nth HR with a porous layer, given by Eq. (25).

In addition to the 1D model previously discussed, this section also shows 3D numerical simulations using finite element method (FEM). In the FEM model, the effective expressions for the complex wavevectors and impedances of each part of the system are used to take into account the viscothermal losses in both the HR and the porous layer. The waveguide and the HRs are considered acoustically rigid using the Neumann boundary condition. A plane wave traveling from the left to the right in the waveguide is also considered. The 3D domain has been meshed with 5456

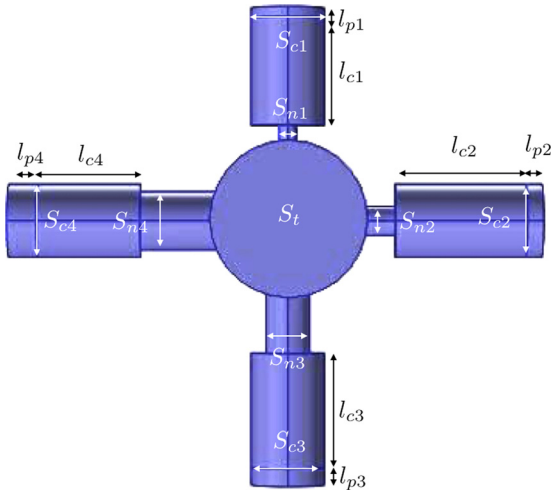

FIG. 7. (Color online) Setup made of 4 HR resonator loaded to a waveguide.

tetrahedral elements. Continuity of the pressure and of the velocity fields is imposed at the interfaces of the porous material and in each change of section in the system. The reflection coefficient is obtained directly from the numerical analysis, and then it is used to evaluate the absorption coefficient which is compared with the one calculated using the 1D analytics.

The dimensions of the HR used in this work are shown in Table II. They are chosen to have their resonant frequencies between 300 and 600 Hz. Dashed line and open circles in Fig. 8(a) represent the analytical and numerical absorption coefficient, respectively, for the whole system considering only the viscothermal losses of the HRs without porous material. In this case, the resulting absorption of the structure is not efficient.

Following the previous procedure, the right amount of porous materials is added to have each HR individually critically coupled (see Fig. 8 for more details). Then, the whole structure is considered (with all the four HRs side loaded) and the reflection coefficient is calculated in the complex frequency plane. The distribution of the zeros of the reflection coefficient is plotted in Fig. 8(b). For this case, Fig. 8(a) shows the analytical (dot dashed line) and numerical (crosses) absorption coefficient. Perfect absorption peaks are present at the frequencies at which the zeros lie at the real frequency axis. The slight differences between the numerical results and the analytical ones are basically due to two

TABLE II. Dimensions of HRs and of the porous material for the broadband absorption. The radius of the waveguide is $S_t = 314\,\text{cm}^2$.

HR 1				HR 2			
l_{n1}	S_{n1}	l_{c1}	S_{c1}	l_{n2}	S_{n1}	l_{c2}	S_{c2}
1.5 cm	0.57 cm^2	8 cm	9.8 cm^2	2.3 cm	1.6 cm^2	10 cm	9.8 cm^2
HR 3				HR 4			
l_{n3}	S_{n3}	l_{c3}	S_{c3}	l_{n4}	S_{n4}	l_{c4}	S_{c4}
4 cm	6.6 cm^2	9 cm	9.8 cm^2	5 cm	5.7 cm^2	8.7 cm	9.8 cm^2

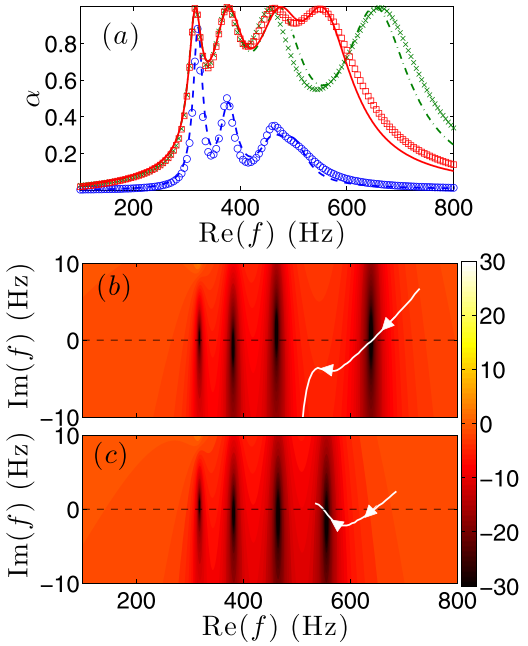

FIG. 8. (Color online) Analysis of the system with four HRs. (a) Absorption coefficient analytically (lines) and numerically (symbols) calculated for each case. Dashed line and open circles represent the absorption coefficient for the configurations without porous material. Dot dashed line and crosses represent the absorption coefficient for the configurations with the 4 HR critically coupled individually. Continuous and open squares represent the absorption coefficient for the case with the 4 HR critically coupled simultaneously covering a broadband range of frequencies. (b) Representation of $20\log|r|$ in the complex frequency plane for the case with the each HR critically coupled individually. In this case the thickness of the porous layer for each HR are $l_{p1} = 0.65\,\text{cm}$, $l_{p2} = 1.15\,\text{cm}$, $l_{p3} = 1.3\,\text{cm}$, $l_{p4} = 3.3\,\text{cm}$. White continuous line represents the trajectory of the zero in the complex frequency plane as the thickness of the porous material is increased. (c) Representation of $20\log|r|$ in the complex frequency plane for the case with broadband absorption with the 4 HRs simultaneously critically coupled. In this case the thickness of the porous layer for each HR are $l_{p1} = 0.65\,\text{cm}$, $l_{p2} = 1.15\,\text{cm}$, $l_{p3} = 1.5\,\text{cm}$, $l_{p4} = 1.9\,\text{cm}$. White continuous line represents the trajectory of the zero in the complex frequency plane as the thickness of the porous material is increased. The pressure distributions at the frequencies with the perfect absorption are shown in Fig. 9.

effects. On one hand, the impedance of the Helmholtz resonators used in the analytical model considers an approximated length correction, which depends on the geometry of the resonator. However, the numerical model considers the real geometry and this can introduce discrepancies with respect to the approximated length correction used in the analytical model. On the other hand, the theory considered here does not take into account the direct interaction of the HRs due to the evanescent coupling but only the indirect through their interference at the waveguide. This direct coupling is inherently considered in the numerical model, so this could also introduce some differences with respect to the theory.

The interaction of the HRs through the interference in the waveguide can be interpreted in the complex frequency plane as an interaction of the poles of the reflection coefficient. Recently, this kind of interference between HRs has been used to generate resonances with high quality factor that can be used to control the acoustic absorption in 1D scattering systems.[27] It is worth it mention here, that the four zeros of the reflection coefficient of the proposed structure

are still on the real frequency axis at the same position as if they were isolated, therefore preserving the perfect absorption condition. This means that the resonance frequency of each resonator is separated enough from its neighbor resonance which results in a weak interaction between them. However, the zero that corresponds to the HR4 is out of the frequency range of our interest. By decreasing the porous material in the HR4, its resonance is shifted to the one of the HR3. Then, one can make use of the interaction between them to have both zeros of the reflection coefficient in the real frequency axis. In more details, as shown in Sec. II (see Fig. 6) if the amount of porous material is increased (decreased) in the resonator, the real part of the zero of the reflection coefficient increases (decreases). Then, if the amount of porous material in HR4 is reduced, its resonant frequency will be shifted to the one of the HR3 and can activate its interaction. First, the trajectory of the zero of the reflection coefficient is analyzed for the case of HR4 side loaded alone to the waveguide. Continuous line in Fig. 8(b) shows the trajectory of the zero of the HR4 when it is isolated from the rest HRs. The arrows show the direction of the trajectory as the porous material is reduced in the HR4. It is worth noting here that the zero of the reflection coefficient of the isolated HR only crosses the real axis at the frequency where it is critically coupled, in good agreement with the zero of the reflection coefficient of the whole configuration.

In order to understand the interaction between HR3 and HR4, the trajectory of the zero of the reflection coefficient that corresponds to the HR4, when all the four HRs are present in the structure, is analyzed [see the continuous line in Fig. 8(c)]. Arrows represent the direction of the trajectory of the zero of the reflection coefficient as the porous material is reduced. Interestingly, as the zero of the HR4 approaches the zero of the HR3, instead of going away from the real axis, it goes back and crosses again the real axis, activating the perfect absorption condition close the to resonance frequency of the HR3. If the reflection coefficient is calculated for the configuration considering the amount of losses in HR4 that produces this crossing near the resonance of the HR3, it results in the color map of Fig. 8(c) (see inset of Fig. 8 for more details about the geometry). It is worth noting here that the presence of HR4 also influences the behavior of HR3, so its losses have also to slightly be modified in order to have the four zeros in the real frequency axis. Figure 8(a) shows the analytical (continuous line) and numerical (open squares) absorption coefficient showing the perfect absorption at the frequencies where the zeros are in the real frequency axis. Thus, the overlap of the four perfect absorption peaks producing a broadband absorption in the frequency range of interest.

In order to visualize the interaction between the HR3 and the HR4, the acoustic field distribution, $|p|$ inside the structure at the frequencies of the perfect absorption peaks is analyzed. Figure 9(a)–9(d) show the acoustic field at the frequencies of the four peaks in the absorption. For the first and second peak, most of the acoustic field is concentrated in the HR1 and HR2, respectively. This proves the weak coupling of the HRs around these frequencies. Thus, in order to achieve perfect absorption, one can consider these HRs as if

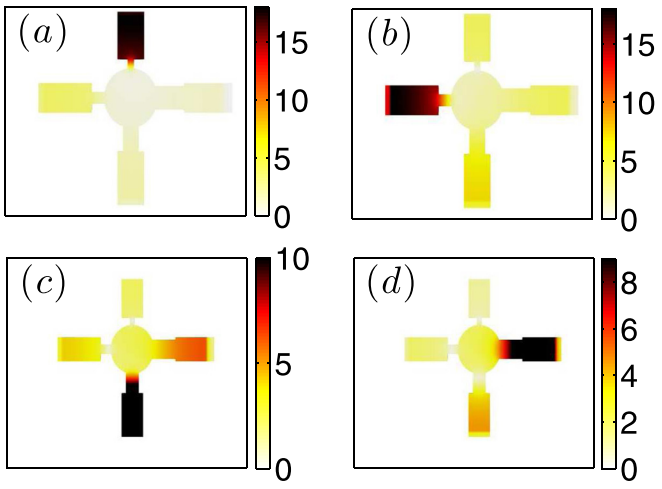

FIG. 9. (Color online) Acoustic field distribution, $|p|$, for the resonances of each HR represented in the case of Fig. 9(c). Acoustic field distribution at frequencies (a) 316, (b) 380, (c) 463, and (d) 554 Hz.

they were isolated. However, looking the acoustic field distribution, $|p|$, around the third and fourth peak, see Figs. 9(c) and 9(d), one can observe that there is a stronger coupling between these HRs since the acoustic field is not only concentrated in the HR3 or in the HR4. At these frequencies, and due to the geometry of the HR3 and HR4, there is stronger coupling between these HRs with the waveguide. In this case, as in the discussion of Eq. (5), the quality factors are small which represent resonances that have larger leakage. This leads to stronger interferences and to an indirect coupling between them.

IV. CONCLUSIONS

The design of broadband and efficient absorbers in the low frequency regime is strongly desired. A plethora of configurations have been proposed during the last years, using ideas from the field of acoustic metamaterials and in particular, using different sub-wavelength resonators, such as coiled slots or Helmholtz resonators (HRs). However, in most of the cases, the obtained configurations were designed only considering the resonant frequency and after that the absorption coefficient is evaluated. In this work, using simple structures and a method of analysis of absorption using the complex frequency plane, the main mechanisms that can lead to perfect and broadband absorption for the problem of low frequency reflection by rigid backed structures are revealed. It is shown that ignoring losses, the reflection coefficient has pairs of pole and zero that are complex conjugate and which have imaginary parts linked to the leakage by radiation. When losses are introduced and balanced by the leakage, critical coupling occurs and leads to total absorption peak. The broadness of this peak is directly related with the strength of the leakage. Once the main mechanisms that lead to single perfect absorption peak are revealed, more complicated structures with multiple critically coupled sub-wavelength resonators are designed. Another important mechanism is revealed in this case, the possible coupling between HRs. Taking all these mechanisms into account,

efficient broadband absorbers in the low frequency regime are obtained.

ACKNOWLEDGMENTS

This work has been funded by the Metaudible project ANR-13-BS09-0003, co-funded by ANR and FRAE.

[1]H. Kuttruff, *Room Acoustics*, 5th ed. (Elsevier, London, UK, 2009), 349 pp.
[2]M. L. Munjal, *Acoustics of Ducts and Mufflers*, 2nd ed. (John Wiley and Sons, Hoboken, NJ, 2014), 416 pp.
[3]J. Kang, *Urban Sound Environment*, 1st ed. (Taylor and Francis, London, UK, 2007), 296 pp.
[4]B. Kotzen and C. English, *Environmental Noise Barriers*, 2nd ed. (Taylor and Francis, London, UK, 2009), 258 pp.
[5]G. Li and C. K. Mechefske, "A comprehensive experimental study of microperforated panel acoustic absorber in MRI scanners," Magn. Reson. Mater. Phys. **23**, 177–185 (2010).
[6]S.-H. Park, "A design method of micro-perforated panel absorber at high sound pressure environment in launcher fairings," J. Sound Vib. **332**(3), 521–535 (2013).
[7]T. J. Cox and P. D'Antonio, *Acoustic Absorbers and Diffusers: Theory, Design and Application*, 2nd ed. (Taylor and Francis, London, UK, 2004), 476 pp.
[8]J. F. Allard and N. Atalla, *Propagation of Sound in Porous Media: Modelling Sound Absorbing Materials*, 2nd ed. (John Wiley and Sons, Hoboken, NJ, 2009), 354 pp.
[9]M. H. Fouladi, M. J. M. Nor, Md. Ayub, and Z. A. Leman, "Utilization of coir fiber in multilayer acoustic absorption panel," Appl. Acoust. **71**, 241–249 (2010).
[10]C. Lagarrigue, J. P. Groby, V. Tournat, and O. Dazel, "Absorption of sound by porous layers with embedded periodic arrays of resonant inclusions," J. Acoust. Soc. Am. **134**(6), 4670–4680 (2013).
[11]J.-P. Groby, W. Lauriks, and T. E. Vigran, "Total absorption peak by use of a rigid frame porous layer backed by a rigid multi-irregularities grating," J. Acoust. Soc. Am. **127**(5), 2865–2874 (2010).
[12]S. Kim, Y. Kim, and J-H. Jang, "A theoretical model to predict the low-frequency sound absorption of a Helmholtz resonator array," J. Acoust. Soc. Am. **119**(4), 1933–1936 (2006).
[13]J. Liu and D. W. Herrin, "Enhancing micro-perforated panel attenuation by partitioning the adjoining cavity," Appl. Acoust. **71**, 120–127 (2010).
[14]C. Wang, L. Huang, and Y. Zhang, "Oblique incidence sound absorption of parallel arrangement of multiple micro-perforated panel absorbers in a periodic pattern," J. Sound Vib **333**, 6828–6842 (2014).
[15]C. Wang and L. Huang, "On the acoustic properties of parallel arrangement of multiple micro-perforated panel absorbers with different cavity depths," J. Acoust. Soc. Am. **130**(1), 208–218 (2011).
[16]S.-H. Park, "Acoustic properties of micro-perforated panel absorbers backed by Helmholtz resonators for the improvement of low-frequency sound absorption," J. Sound Vib. **332**(20), 4895–4911 (2013).
[17]X. Cai, Q. Guo, G. Hu, and J. Yang, "Ultrathin low-frequency sound absorbing panels based on coplanar spiral tubes or coplanar Helmholtz resonators," Appl. Phys. Lett. **105**, 121901 (2014).
[18]S. M. Ivansson, "Anechoic coatings obtained from two- and three-dimensional monopole resonance diffraction gratings," J. Acoust. Soc. Am. **131**(4), 2622–2637 (2012).
[19]J. Wen, H. Zhao, L. Lv, B. Yuan, G. Wang, and X. Wen, "Effects of locally resonant modes on underwater sound absorption in viscoelastic materials," J. Acoust. Soc. Am. **130**(3), 1201–1208 (2011).
[20]H. Meng, J. Wen, H. Zhao, L. Lv, and X. Wen, "Analysis of absorption performances of anechoic layers with steel plate backing," J. Acoust. Soc. Am. **132**(1), 69–75 (2012).
[21]J. Wang, P. Leistner, and X. Li, "Prediction of sound absorption of a periodic groove structure with rectangular profile," Appl. Acoust. **73**, 960–968 (2012).
[22]H. V. Fuchs and X. Zha, "Micro-perforated structures as sound absorbers-A review and outlook," Acta Acust. Acust. **92**, 139–146 (2006).
[23]G. Theocharis, O. Richoux, V. Romero García, A. Merkel, and V. Tournat, "Limits of slow sound propagation and transparency in lossy, locally resonant periodic structures," New J. Phys. **16**, 093017 (2014).
[24]J.-P. Groby, W. Huang, A. Lardeau, and Y. Auregan, "The use of slow waves to design simple sound absorbing materials," J. Appl. Phys. **117**, 124903 (2015).
[25]P. Wei, C. Croënne, S. Chu, and J. Li, "Symmetrical and anti-symmetrical coherent perfect absorption for acoustic waves," Appl. Phys. Lett. **104**, 121902 (2014).
[26]G. Ma, M. Yang, S. Xiao, Z. Yang, and P. Sheng, "Acoustic metasurface with hybrid resonances," Nat. Mater. **13**, 873–878 (2014).
[27]A. Merkel, G. Theocharis, O. Richoux, V. Romero-García, and V. Pagneux, "Control of acoustic absorption in 1D scattering by indirect coupled resonant scatterers," Appl. Phys. Lett. **107**, 244102 (2015).
[28]P. H. Smith, "Transmission line calculator," Electronics **12**, 29–31 (1939).
[29]P. H. Smith, "An improved transmission line calculator," Electronics **17**, 130–133, 318–325 (1944).
[30]S. Ramo, J. R. Whinnery, and T. Van Duzer, *Fields and Waves in Communications Electronics*, 3rd ed. (John Wiley and Sons, Hoboken, NJ, 1965), pp. 235–239.
[31]V. Romero-García, G. Theocharis, O. Richoux, A. Merkel, V. Tournat, and V. Pagneux, "Perfect and broadband acoustic absorption by critical coupling," Sci. Rep. **6**, 19519 (2016).
[32]O. Richoux and V. Pagneux, "Acoustic characterization of the Hofstadter butterfly with resonant scatterers," Europhys. Lett. **59**, 34–40 (2002).
[33]V. Pagneux, "Trapped modes and edge resonances in acoustics and elasticity," in *Dynamic Localization Phenomena in Elasticity, Acoustics and Electromagnetism, CISM International Centre for Mechanical Sciences* (Springer, Vienna, Austria, 2013), Vol. 547, 181–223.
[34]C. Zwikker and C. W. Kosten, *Sound Absorbing Materials* (Elsevier, New York, 1949), 174 pp.
[35]V. Dubos, J. Kergomard, D. Keefe, J. P. Dalmont, A. Khettabi, and K. Nederveen, "Theory of sound propagation in a duct with a branched tube using modal decomposition," Acta Acust. Acust. **85**(2), 153–169 (1999).
[36]J. Kergomard and A. Garcia, "Simple discontinuities in acoustic waveguides at low frequencies: Critical analysis and formulae," J. Sound Vib. **143**(3), 465–479 (1987).
[37]P. Rebillard, J.-F. Allard, C. Depollier, and P. Guignouard, "The effect of a porous facing on the impedance and the absorption coefficient of a layer of porous material," J. Sound Vib. **156**, 541–555 (1992).